Int. J. Electrochem. Sci., 16 **(2021)** Article ID: 210621, doi: 10.20964/2021.06.46

International Journal of
ELECTROCHEMICAL
SCIENCE
www.electrochemsci.org

Study on Electrochemical Corrosion Behavior of 13Cr Steel (0Cr13Ni2P) in Saturated CO_2 Solution

*Qiu Li Zhang, Zi Yue Song**, *WenZhi Liao, ZhaoYang Chen, Jun Zhou*

School of Chemistry and Chemical Engineering, Xi'an University of Architecture and Technology, Xi'an, China
*E-mail: 1206118357@qq.com

Received: 16 February 2021 / *Accepted:* 6 April 2021 / *Published:* 30 April 2021

A type of 13Cr Steel (0Cr13Ni2P) was selected in this paper as a research object. The corrosion behavior of this 13Cr steel in the CO_2 environment were studied by means of electrochemical testing technology, and the effects of Cl-, temperature and other factors on the corrosion behaviors were investigated. There was an obvious passivation region in the 13Cr steel when immersed in NaCl solution saturated with CO_2, and the AC impedance spectrum was characterized by dual capacitive arc. The addition of CO_2 reduced the charge transfer resistance and the passive film resistance, and increased the corrosion rate significantly. The increase of the temperature and Cl^- concentration had no effect on the characteristics of EIS. The composition of the passivation film on the surface of 13Cr steel was analyzed by XPS, the passive film is n-p type semiconductor. With the increase of the potential of forming passive film, the steady-state current density was decreased, the donor density and acceptor density of passive film was decreased, and the protection performance was improved.

Keywords: 13Cr steel; saturated CO_2; polarization; electrochemical corrosion

1. INTRODUCTION

With the development of the petroleum industry and the increasing demand for oil and gas resources, the working depth of the oil and gas fields is gradually developing, and the working conditions are getting worse and worse. The CO_2 corrosion of oil and gas well pipeline steel has become a very serious problem, and the corrosive environment can lead to local or overall corrosion of pipeline steel[1].

Chromium can promote the formation of the passive film on the surface of the stainless steel, protect the substrate and endow it with strong resistance to CO_2 corrosion.13Cr Steel with 13% Cr is a kind of alloy steel with a martensitic microstructure, which is widely used in oil and gas fields containing CO_2.13Cr stainless-steel pipe is a kind of oil pipeline steel with good corrosion resistance, the application of 13Cr Steel in high-temperature and high-pressure (HTHP) oil and gas wells with high CO_2 content is increasing[2].JFE and NKK of Japan and Tenaris of Argentina have done a lot of work in the development and application of oil pipelines. JFE company launched a series of martensitic stainless-steel tubing, such as common 13Cr, super 13Cr and high strength 15Cr, which are used in the humid environment containing CO_2 in recent 20 years. Common 13Cr and super 13Cr stainless steel tubing have been widely used in Europe, North America and other regions to solve CO_2 corrosion in the mining process[3].

At present, 13Cr martensitic stainless-steel has been used in the oil and gas industries. However, 13Cr stainless steel is still faced with CO_2 corrosion. The corrosion behaviors of the chromium-containing steel in the CO_2 environment were extensively studied[4-15]. The main factors affecting the CO_2 corrosion of 13Cr Steel include temperature, CO_2 partial pressure, flow rate and Cl^- concentration[16]. Many researchers investigated the corrosion behaviors of the 13Cr alloy pipes[17-21]. Li studied the stress and crevice corrosion behaviors of the 13Cr stainless-steel in 3.5wt.% NaCl solution. The applied stress degraded the passive film, and resulted in the negative shift of the pitting potential and the enhancement of pitting sensitivity. The crevice corrosion of the 13Cr stainless-steel was divided into induction period, rapid development period and stable development period[22]. Xiao studied the corrosion of the 13Cr steel in the high-temperature steam environment, and the corrosion rate was less than 0.04 mm/a, which was mainly affected by temperature and Cl^- concentration. High temperature inhibited steam condensation and the compactness of the Cr-rich layer, and Cl^- affected the activity of the Fe atoms in the metal matrix[23].

The depth and temperature of the wells will be further improved in the future production process of oil and gas wells, and the corrosion environment will be more complex and severe. The corrosion resistance of Cr-containing low alloy steel is difficult to meet the requirements, and the oil casing steels with better corrosion resistance are required. The 13Cr steel (0Cr13Ni2P) was developed by Henan Zhengzhou Yongtong Special Steel Co. Ltd., which was produced by adding a small amount of alloy in the smelting process. This 13Cr steel is equipped with a superior cost-performance ratio and broad application prospect in the fields of oil and gas. However, there are little researches on the corrosion of this 13Cr steel in the CO_2 environment. Herein, the influence of Cl^- concentration, temperature and other factors on the CO_2 corrosion behaviors of the 13Cr steel was studied by electrochemical testing technologies. The composition and structure of the corrosion products were analyzed by XPS under simulated conditions, which provided the necessary theoretical basis for the research and application of the new steel in future oil and gas field development.

2. EXPERIMENTS

2.1. Materials

The 13Cr steel produced by Zhengzhou Yongtong Special Steel was used in this paper, and the chemical composition is shown in Table 1. The sample was processed into a working electrode of 10 mm × 10 mm × 2 mm. The steel was welded to the copper wire and wrapped with epoxy resin, left a working area of $1cm^2$. The working surface was sequentially polished with sandpaper of #240 to #1500, used acetone and deionized water to clean. Finally, wiped the working electrode with anhydrous ethanol, dried and placed in the drying oven for standby.

Table 1. Chemical composition in wt.% of the material.

Element	C	Si	Mn	P	S	Cr	Mo	Ni	Al	Fe
0Cr13Ni2P	0.097	0.43	0.65	0.083	0.0044	13.9	0.001	1.82	0.0032	Bal

2.2 Experimental conditions and procedure

NaCl solution was selected as the electrolyte in the electrochemical test. All experiments were carried out at room temperature (about 25℃) in 3.50wt.% NaCl solution except for special instructions. Before the experiment, N_2 was used to remove O_2 for 2 hours, and then CO_2 was added to reach saturation. CO_2 was continuously added during the experiment, and the test temperature was controlled by the constant temperature oil bath. The traditional three electrode system was used for electrochemical measurement (the 13Cr steel as a working electrode, high-purity graphite with a large surface area was used as a counter electrode, and reference electrode was saturated silver chloride electrode) on Correst CS2350 electrochemical workstation from Wuhan. All the potentials in this paper were based on the saturated silver chloride electrode.

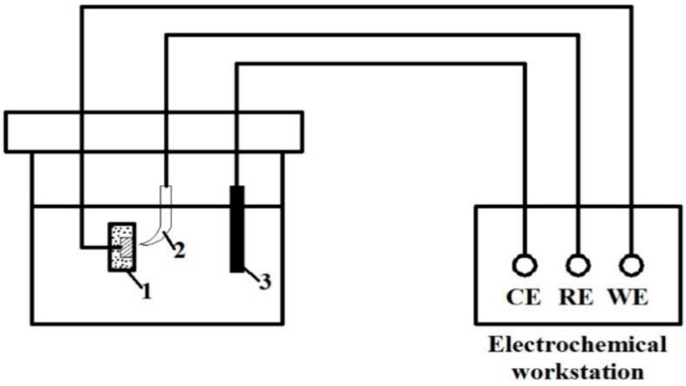

Figure 1. Schematic diagram of electrochemical device (1-13Cr steel,2-Saturated silver chloride electrode,3-High-purity graphite electrode)

Before the measurement, pre-polarized the working electrode for 5 minutes at -1.2 V. Then, immersed the working electrode in the test solution for 0.5 hours until the system was stable for open circuit potential measurement. AC impedance spectroscopy under the open circuit potential was obtained for 0.5 hours under the following conditions (the frequency range was 100kHz to 10mHz, the perturbing AC amplitude was 5mV, the logarithm scanning was 10 times, and the frequency was at 10). The polarization curves were recorded at specific parameters (the potential range was -0.2V ~ +1.0V (vs. open circuit potential), and the scan rate was 0.33mV/s). Cview analysis software was used for data fitting analysis of potentiodynamic polarization curves, and ZsimpWin software was employed to fit the electrochemical impedance spectroscopy test data.

The passive films formed on metals are known to exhibit a semiconducting behavior, Mott-Schottky measurements were used to study the semiconducting properties of the film[24]. The M-S curve was measured until open circuit potential was stable. The measured potential range is -0.6V~+0.1V, the scanning rate was 50mV/s, and the test frequency was 1000 Hz.

The composition of the corrosion products was analyzed using X-ray Photoelectron Spectroscopy. All the testing samples were scraped off from the corrosion samples for XPS test. The chemical composition of passive films on the 13Cr steels was characterized by Al Kα(1486.6 eV) at 150W(15kv, 10mA). The binding energies of XPS spectra were calibrated with reference to the C1s at 284.8eV for adjusting the shifted charge. XPSPEAK version 4.1 was used for peak fitting and a linear baseline was used for background subtraction.

3. RESULTS AND DISCUSSION

3.1 Effect of CO_2

The potentiodynamic polarization curves of the 13Cr steel in the 3.5wt.% NaCl solution under the N_2 or CO_2 atmosphere are shown in Fig. 2. The 13Cr steel was directly passivated under the N_2 or CO_2 atmosphere, and there was no activation-passivation intermediate state. The pitting occurred when the potential reached a critical value, and the difference of the pitting potential under different atmospheres was not obvious. The addition of CO_2 had little effect on the pitting sensitivity of the 13Cr steel in NaCl solution. In the N_2 atmosphere, there was an obvious Tafel zone in the polarization curve, and the Tafel zone disappeared with the addition of CO_2, indicating that CO_2 improved the possibility of the films' formation.

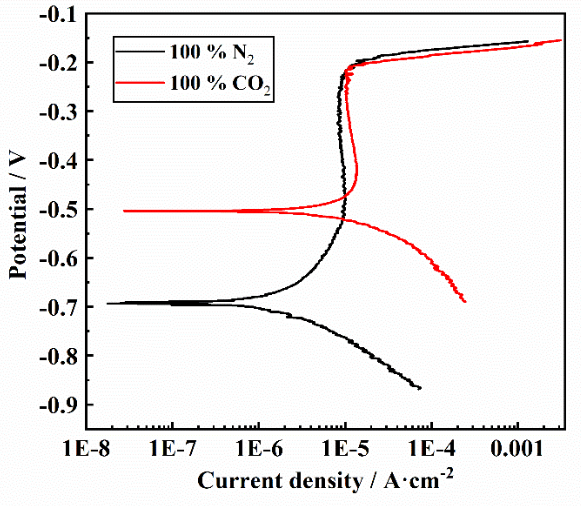

Figure 2. Potentiodynamic polarization curves of 13Cr steel in the 3.5wt.% NaCl solution under the N_2 or CO_2 atmosphere.

The excessive adsorption of Cl^- in the pure nitrogen environment increased the active dissolution area, and reduced the possibility of the passivation film formation. However, the lack of depolarizer after pre-deoxygenation of the solution makes it difficult to form a passive film. The depolarizer was introduced to the system by CO_2, and the possibility of the film formation was increased. By comparing the passivation current density of the two passivation regions under the N_2 or O_2 atmosphere, the passivation current density was higher in the saturated CO_2 environment, which indicated that the addition of CO_2 reduced the protection performance of the passive film in the passivation region. The cathode Tafel slope of the 13Cr steel in the saturated CO_2 environment is larger than that in the pure N_2 environment, which indicated that the cathodic reaction rate of the 13Cr steel in the CO_2 saturated environment is higher.

The AC impedance spectra of the 13Cr steel in the 3.50wt.% NaCl solution under the N_2 or CO_2 atmosphere are shown in Fig. 3. Hua indicated that the increase of CO_2 has little effect on the general corrosion of the steel[25]. From Fig 3., the characteristics of AC impedance spectra in the N_2 or CO_2 atmosphere were similar, which illustrated that CO_2 did not change the corrosion mechanism. CO_2 significantly reduced the radius of the capacitive arc, which indicated that in the early stage of corrosion CO_2 significantly reduced the protective performance of the corrosion product film on the substrate and accelerated the corrosion rate.

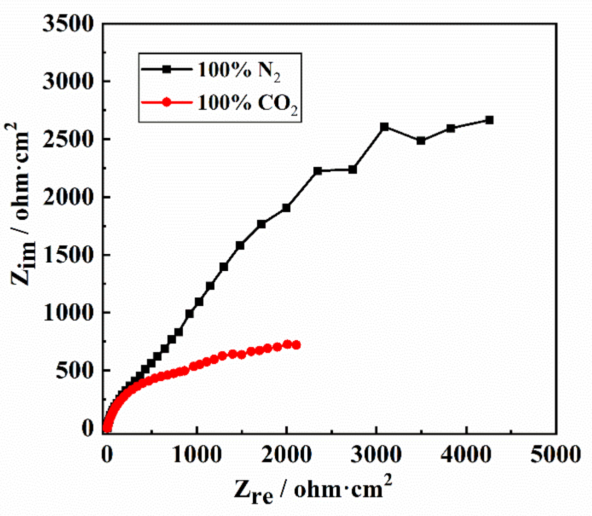

Figure 3. EIS of 13Cr Steel in the 3.50wt.% NaCl solution under the N_2 or CO_2 atmosphere.

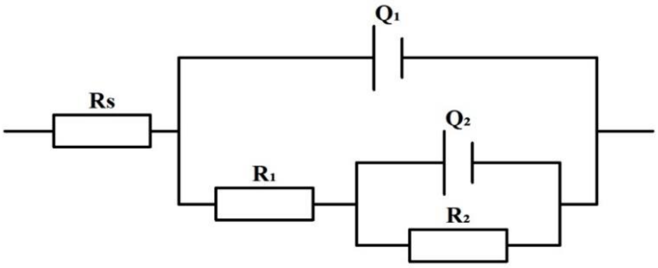

Figure 4. Equivalent circuit model for EIS fitting.

The equivalent circuit is shown in Fig. 4, which was used to fit the EIS of the 13Cr steel in the 3.50wt.% NaCl solution under the N_2 or CO_2 atmosphere. Where R_S represents the solution resistance, Q_1 and Q_2 refer to the electric double-layer capacitance and passivation film capacitance respectively, R_1 and R_2 represent the charge transfer resistance and passivation film resistance respectively. The fitting results are shown in Table 2.

Table 2. Fitting results of EIS of 13Cr Steel in the 3.50wt.% NaCl solution under the N_2 or CO_2 atmosphere.

solution environment	$R_S/\Omega{\bullet}cm^2$	$Q_1/F{\bullet}cm^{-2}$	$R_1\Omega{\bullet}cm^2$	$Q_2/F{\bullet}cm^{-2}$	$R_2/\Omega{\bullet}cm^2$
N_2	2.467	0.00032	1526	0.00082	6882
CO_2	1.978	0.00039	1493	0.0038	1429

CO_2 dissolves in water and combines with water to form carbonic acid, which releases H^+ after ionization. The reaction is as follows[26-29]:

$H_2CO_3 \rightarrow H^+ + HCO_3^-$ (1)

$HCO_3^- \rightarrow H^+ + CO_3^{2-}$ (2)

The addition of CO_2 increased the concentration of H^+, decreased the pH of the solution and provided cathodic species for reaction with the steel surface[30]. On the one hand, the increase of the solution acidity led to the increase of the ionic conductivity of the passivation film, resulting in the decrease of the stability of the passivation film[31]. On the other hand, in CO_2 environment, the dehydroxylation effect of H_2CO_3 on the passivation film led to the decrease of the stability of the passive film on the 13Cr steel surface, accelerating the destruction process of the passivation film[32-33].

3.2 Effect of Cl-

The potentiodynamic polarization curves of the 13Cr steel in the saturated CO_2 solution with different Cl^- concentrations are shown in Fig. 5. Used NaCl to adjust the Cl^- concentration to 1.75wt.%, 3.50wt.%, 7.00wt.%, 10.50wt.%, 14.00wt.%. The 13Cr steel directly entered the passivation zone in the solutions with different Cl^- concentrations, and there were no obvious activation-passivation transition characteristics. Some researchers found that the presence of a small amount of Cl^- can significantly reduce the passivation tendency of steel, and the CO_2 corrosion rate of carbon steel decreases sharply with the increase of salt concentration[34]. NaCl improves the conductivity of saturated CO_2 solution, resulting in the rapid dissolution of protective film on steel surface[35]. Xiao indicated that the enhance of the Cl^- concentration led to the conductivity of the solution raised, and the adsorption of Cl^- on the sample surface also increased[23,36]. The possibility of the reaction between chloride ion and iron ion increases, which promotes the active dissolution of iron. Along with the increase of the Cl^- concentration, the passivation range decreased significantly, the passivation current density increased, and the pitting potential decreased significantly, which meant that the pitting sensitivity of the material increased. Cl^- reduced the stability of the passivation film on the surface of the 13Cr steel and the pitting resistance.

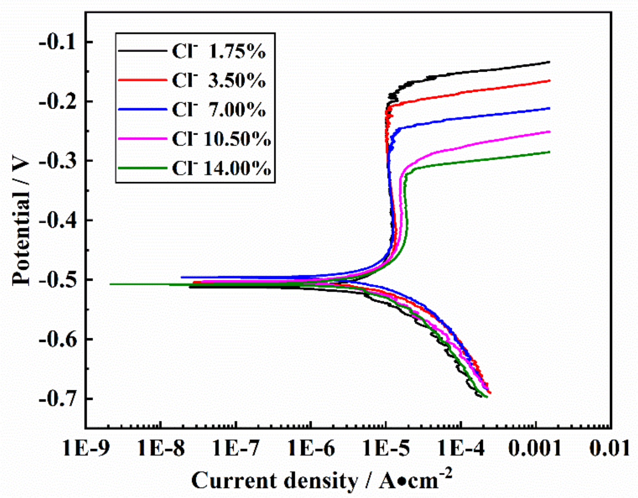

Figure 5. Potentiodynamic polarization curves of 13Cr Steel in the saturated CO_2 solution with different Cl^- concentration.

Fitted the potentiodynamic polarization curves, the results are shown in Table 3. E_{corr} represents the corrosion potential, and I_{corr} represents the corrosion current density. The E_{corr} value first increased and then decreased in pace with the increase of the Cl^- concentration, which indicated that the low concentration of Cl^- increased the corrosion tendency of the 13Cr steel in NaCl solution saturated with CO_2, while the high concentration of Cl^- reduced the corrosion tendency. The I_{corr} value first increased and then decreased with the increase of the Cl^- concentration, and reached the maximum when the concentration of NaCl was 10.50%. In low-concentration Cl^- solution, the increase of the Cl^- accelerated the corrosion rate of the 13Cr steel, while Cl^- inhibited the corrosion process when the Cl^- concentration reached a certain critical value. Schmitt showed that increasing Cl content to a certain value can inhibit CO_2 corrosion by reducing the solubility of CO_2 in solution at room temperature[37].

Table 3. Potentiodynamic polarization curve fitting results of 13Cr steel in the saturated CO_2 solution with different Cl^- concentration.

Cl^- %	I_{coor}/A·m^{-2}	E_{coor}/V
1.75	1.173E-5	-0.513
3.50	1.784E-5	-0.504
7.00	1.985E-5	-0.496
10.50	2.766E-5	-0.503
14.00	2.074E-5	-0.506

Fig. 6 shows the impedance spectra of 13Cr steel in the saturated CO_2 solution with different Cl^- concentration. There was no change in the shape characteristics of the EIS spectra with the increase of the Cl^- concentration. EIS was composed of capacitive arc in the medium/high-frequency region and capacitive arc in the low-frequency region under different Cl^- concentrations, which indicated that the change of the Cl^- concentration did not change the corrosion mechanism of the 13Cr steel in the saturated CO_2 solution.

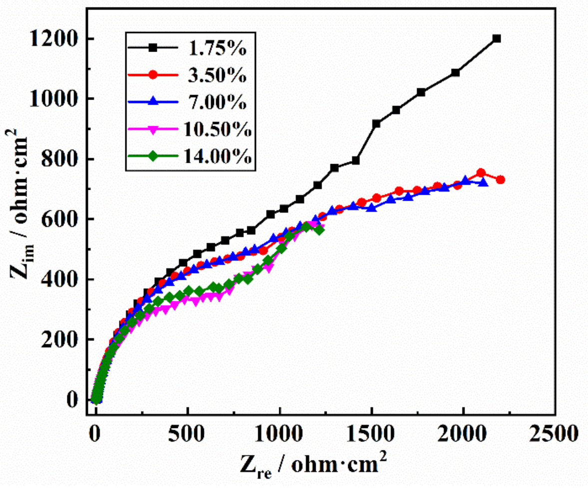

Figure 6. EIS of 13Cr steel in the saturated CO_2 solution with different Cl^- concentration.

There was no inductive arc in the solution with all Cl^- concentration, which was due to the fact that the compact and complete $Cr(OH)_3$ passivation film was formed on the surface of the 13Cr steel with a high rate of anodic reaction ($Cr + 3OH^- \rightarrow Cr(OH)_3 + 3e$)and good protection ability for the substrate.

Because of the rough surface of the sample and the dispersion effect, the constant phase angle elements Q_1 and Q_2 were used to replace the electric double-layer capacitance and passivation film capacitance respectively in the equivalent circuit. The impedance of the element with constant phase angle can be expressed as follows:

$$Z = \frac{1}{(jwY_0)^n}$$

Where Y_0 and N are the two parameters of Q, Y_0 and capacitance have the same dimension. The n is the dispersion index with dimensionless, and the value range is 0～1. The circuit diagram shown in Fig. 4 was used for fitting, and the fitting results are shown in Table 4.

Table 4. Fitting results of EIS of 13Cr steel in the saturated CO_2 solution with different Cl^- concentration.

Cl^- %	$R_S/\Omega\bullet cm^2$	$Q_1/F\bullet cm^{-2}$	n_1	$R_1\Omega\bullet cm^2$	$Q_2/F\bullet cm^{-2}$	n_2	$R_2/\Omega\bullet cm^2$
1.75	3.553	0.00039	0.7434	1700	0.0034	0.8693	2673
3.50	1.978	0.00034	0.7391	1493	0.0038	0.0821	1429
7.00	1.358	0.00032	0.7378	1455	0.0042	0.8745	1377
10.50	1.338	0.00021	0.8225	763	0.0022	0.7102	1702
14.00	1.307	0.00021	0.8130	889	0.0024	0.7762	1827

It can be seen from Table 4 that the charge transfer resistance and passive film resistance first decreased and then increased with the increase of the Cl^- concentration. The low concentration of Cl^- promoted the corrosion of the 13Cr steel, while the high concentration of Cl^- inhibit the corrosion of the 13Cr steel. The fitting results are consistent with the polarization curves.

In the NaCl solution saturated with CO_2, the following reactions mainly occurred at the cathode[37-39]:

$$2H_2CO_3 + 2e \rightarrow H_2 + 2HCO_3^- \tag{3}$$

$$2H^+ + 2e \rightarrow H_2 \tag{4}$$

The main reactions of anode were as follows:

$$Fe + Cl^- + H_2O \rightarrow [FeCl(OH)]_{ad}^- + H^+ + e \tag{5}$$

$$[FeCl(OH)]_{ad}^- \rightarrow FeClOH + e \tag{6}$$

$$FeClOH + H^+ \rightarrow Fe^{2+} + Cl^- + H_2O \tag{7}$$

When the content of Cl^- was low, Cl^- promoted the anodic activation dissolution of the metals through the intermediate corrosion product ($[FeCl(OH)]_{ad}^-$). The catalytic effect was enhanced with the increase of the Cl^- concentration. Therefore, the corrosion rate increased with the increase of Cl^- concentration at the low content of Cl^-. The corrosion rate was accelerated at the high concentration of Cl^-, $FeCO_3$ in the solution was quickly saturated to form the corrosion product film, which played a role in protecting the matrix, thus reducing the corrosion rate. Moreover, when the solution contains Cl^- and other anions, if the content of Cl^- is relatively high, Cl^- is preferentially adsorbed on the metal surface. The chance of H^+, H_2CO_3 and HCO_3^- participating in the reaction is reduced, which reduces the CO_2 corrosion rate[39].

3.3 Effect of temperature

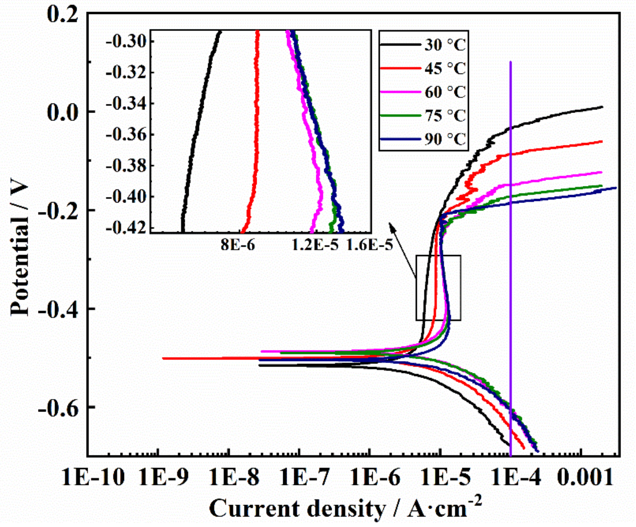

Figure 7. Polarization curves of 13Cr steel in the 3.50wt.% NaCl solution saturated with CO_2 at different temperature.

The polarization curves of 13Cr steel in the 3.50wt.% NaCl solution saturated with CO_2 at different temperature are shown in Fig. 7. The 13Cr steel was passivated at all test temperatures. The passivation current density increased with the increase of the temperature in the range of 30~90°C, and the protection performance of the passivation film decreased. The passivation current density did not change significantly when the temperature increased from 75°C to 90°C. The pitting behaviors of the 13Cr steel occurred in the range of 30~90°C. The rate of pitting expansion also increased with the increase of the temperature. When the temperature reached 90°C and the potential reached the critical pitting potential, the corrosion current density increased rapidly. The potential corresponding to the current density of 100μA/cm^2 was taken as the pitting potential. The pitting potential decreased with the increase of the temperature, which indicated that the pitting sensitivity of the 13Cr steel was increased by increasing the temperature in the 3.50wt.% NaCl solution saturated with CO_2.

The increase of temperature increases the kinetics of chemical reaction in general. On the contrary, if the corrosion rate is limited by the dense surface oxide film, the corrosion rate is expected to decrease with the increase of temperature[40]. The electrochemical impedance spectra of the 13Cr steel in the 3.50wt.% NaCl solution saturated with CO_2 at different temperature are shown in Fig. 8. The temperature in the range of 30~90°C did not change the shape characteristics of EIS. When the temperature increased from 30°C to 75°C, the radius of the capacitive arc in the high-frequency region decreased significantly. When the temperature increased from 75°C to 90°C, the radius of capacitive arc in the high-frequency region increased slightly. The corrosion rate of the new 13Cr steel was increased by increasing temperature, but the corrosion rate was inhibited when the temperature reached 90°C. The results were consistent with the polarization curves.

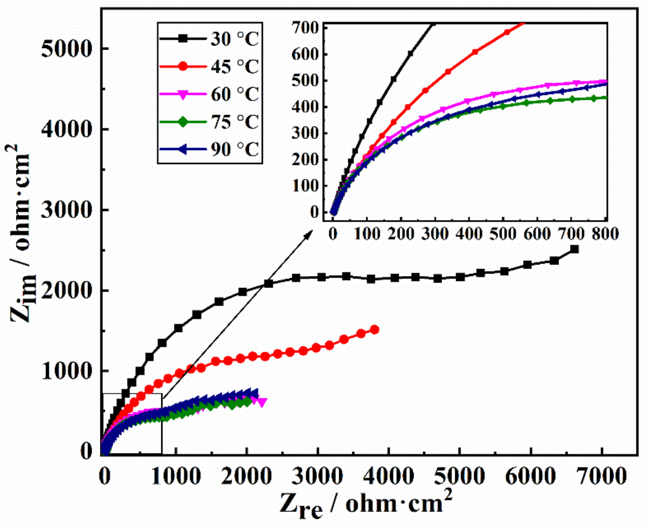

Figure 8. EIS of 13Cr steel in the 3.50wt.% NaCl solution saturated with CO_2 at different temperature.

The fitting circuit in Fig. 4 was used to fit the EIS of 13Cr Steel in the 3.50wt.% NaCl solution saturated with CO_2 at different temperature, and the fitting results are shown in Table 5. The charge transfer resistance and the passive film resistance decreased first and then increased with the increase of the temperature. The higher polarization resistance near 75°C indicates that the corrosion rate decreases sharply and the steel is protected by corrosion product film[41]. Both the charge transfer resistance and the passive film resistance reached the minimum value at 75°C. The temperature in the range of 30~75°C destroyed the stability of the passivation film, thus reducing the protective effect on the substrate and increasing the corrosion rate. In Yue's research, dense and uniform passivation film was formed on 13Cr steel in saturated CO_2 environment at 90°C, which reduced the corrosion rate of 13Cr steel[13]. When the temperature rose to 90°C, the protective performance of the passivation film on the substrate increased and the corrosion rate decreased. The results were consistent with the potentiodynamic polarization curves.

Table 5. Fitting results of EIS of 13Cr steel in the 3.50wt.% NaCl solution saturated with CO_2 at different temperature

T/°C	R_S/Ω•cm^2	Q_1/F•cm^{-2}	n_1	R_1/Ω•cm^2	Q_2/F•cm^{-2}	n_2	R_2/Ω•cm^2
30	0.789	0.000179	0.8148	5858	0.00423	0.9998	3245
45	2.420	0.000211	0.7898	3342	0.00412	0.8757	2482
60	4.361	0.000250	0.7871	1360	0.00377	0.8110	1421
75	2.265	0.000284	0.7690	1209	0.00404	0.8223	1316
90	1.978	0.000340	0.7391	1493	0.00387	0.8216	1429

In the range of 70~90°C, the CO_2 corrosion rate reached the maximum, and the increase of the temperature reduced the corrosion rate, which was attributed to the denser corrosion product film formed in the high-temperature environment and the stronger protection of the substrate. With the increase of the temperature, the anodic reaction rate increased, and the corrosion product film was easy to form and more compact, which prevented the anodic dissolution of the matrix. Under the combined action of these two factors, the corrosion rate first increased and then decreased.

3.4 Study on passivation film performance of 13Cr steel in the CO_2 environment

3.4.1 Effect of film potential on the performance of passive film

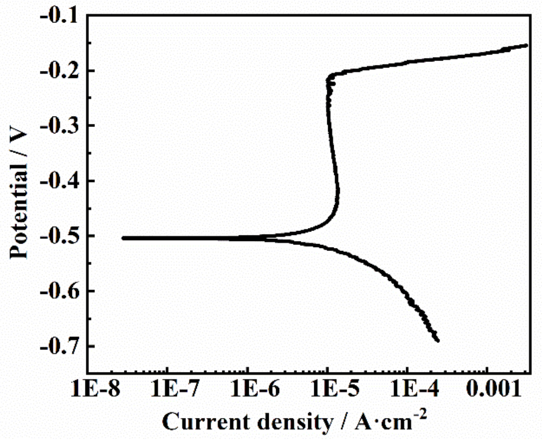

Figure 9. Potentiodynamic polarization curve of 13Cr steel in 3.50wt.% NaCl solution saturated with CO_2 at 90℃.

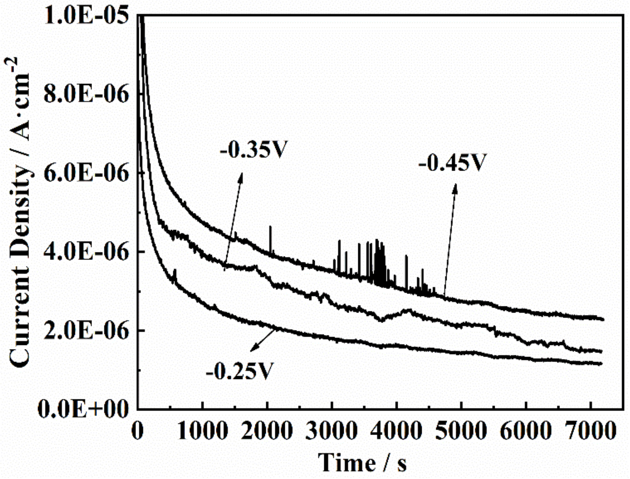

Figure 10. Potentiostatic polarization curves of 13Cr Steel in 3.50wt.% NaCl solution saturated with CO_2 at different potentials.

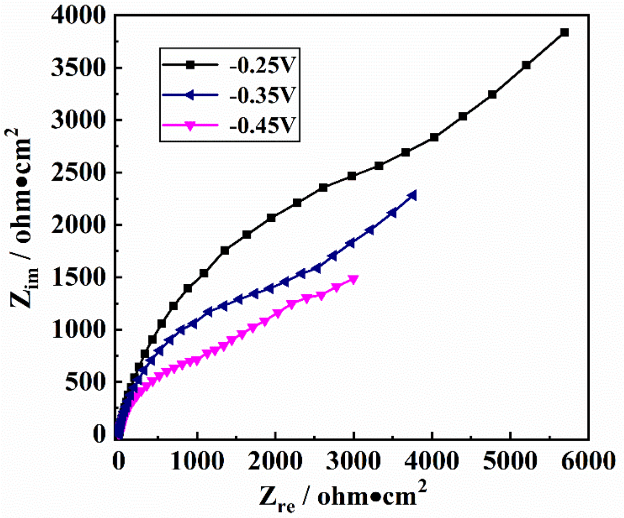

Figure 11. EIS of passive film on 13Cr Steel in 3.50% NaCl solution saturated with CO_2 at different potentials.

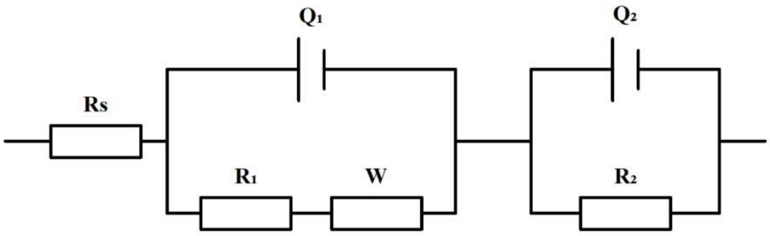

Figure 12. EIS fitting circuit of passive film on 13Cr Steel in 3.50% NaCl solution saturated with CO_2 at different potentials.

Fig. 9 shows the potentiodynamic polarization curve of 13Cr Steel in 3.50wt.% NaCl solution saturated with CO_2 at 90℃. There was an obvious passivation zone (-0.45~-0.2V), the passivation current density was 1.13E-5 A·cm^{-2}. At this time, the dense passivation film was formed on the surface of the sample.

Fig. 10 shows the potentiostatic polarization curves of the 13Cr steel in 3.50% NaCl solution saturated with CO_2 at different potentials. The steady-state current density of the passive film presented a downward trend with the increase of the film potential, indicated that the passivation film formed at the high potential had better protection performance for the material matrix. Moreover, the passivation current density decreased with the increase of the passivation time, which illustrated that the protection performance of the passivation film was improved by prolonging the film formation time.

Fig. 11 shows the electrochemical impedance spectra of the passivation film of the 13Cr steel in 3.50% NaCl solution saturated with CO_2 at different potentials. The electrochemical impedance spectra of the passivation films formed at different potentials were composed of capacitive arc at high-frequency region and Warburg impedance at low-frequency region, which indicated that the control steps were change from activation control to diffusion control in the whole electrode process. The formation of diffusion resistance is due to the formation of the passivation film hindering the charge diffusion channel. The radius of the capacitive reactance arc increased with the increase of the film potential[42].

Table 6. Fitting results of EIS of passivation film formed on 13Cr steel in 3.50wt.% NaCl solution saturated with CO_2 at different potentials.

Potential/ V	R_S/ Ω•cm^2	Q_1/ F•cm^{-2}	n_1	R_1/ Ω•cm^2	Y_W/ H^{-1}•S$^{-0.5}$	Q_2/ F•cm^{-2}	n_2	R_2/ Ω•cm^2
-0.45	2.229	2.796E-4	0.8258	1377	1.58E-3	9.278E-4	0.5885	4.562
-0.35	1.641	3.601E-4	0.864	2219	1.32E-3	1.392E-3	0.6558	5.261
-0.25	2.606	3.156E-4	0.8614	3821	8.43E-4	3.478E-5	0.5398	6.21

Fig. 12 shows the fitting circuit diagram of the electrochemical impedance spectra of the passivation film of the 13Cr steel in 3.50wt.% NaCl solution saturated with CO_2 at different potentials, where R_S represents the solution resistance, Q_1 and R_1 refer to the capacitance and resistance of the passive film respectively, w represents the diffusion impedance, and Q_2 and R_2 stand for the electric double-layer capacitance and charge transfer resistance respectively. The fitting results are shown in Table 6. The charge transfer resistance and the passive film resistance increased with the positive shift of the film potential, which indicated that the resistance of the transfer of the charge in the passivation film increased, the density and stability of the passivation film increased, and the corrosion resistance of the passivation film increased. At the same time, the diffusion coefficient decreased and the diffusion impedance increased with the increase of the film potential, indicating that the protective effect of the passivation film on the substrate was enhanced.

The passivation film on the stainless-steel surface usually has semiconductor properties[43,44]. In general, the semiconductor characteristics of the passivation film can be described by Motto-Schottky relation. For n-type semiconductor, Motto-Schottky relation is as follows:

$$\frac{1}{C^2}=\frac{2}{\varepsilon\varepsilon_0 eN_D}(E-E_{fb}-\frac{KT}{e})$$

For p-type semiconductors, the Mott-Schottky relation is as follows:

$$\frac{1}{C^2} = \frac{2}{-\varepsilon\varepsilon_0 e N_A}(E - E_{fb} - \frac{KT}{e})$$

Among them, ε_0 is 8.85419×10^{-14} F/cm represents the vacuum dielectric constant, ε is the semiconductor dielectric constant (15.6 F/cm in this paper), e is the electron charge, N_D and N_A are the donor density and acceptor density respectively, E is the applied voltage, E_{fb} is the flat band potential, K is the Boltzmann constant, and T is the absolute temperature. Therefore, the type of the semiconductor can be judged by measuring the capacitance of the space charge layer under different potentials and plotting the potential E with C^{-2}. The passivation film is p-type semiconductor when the slope of the C^{-2}-E linear region is negative, the passivation film n-type semiconductor when the slope of the C^{-2}-E linear region is positive, it. The donor density N_D and acceptor density N_A can be obtained from the slope of the linear equation.

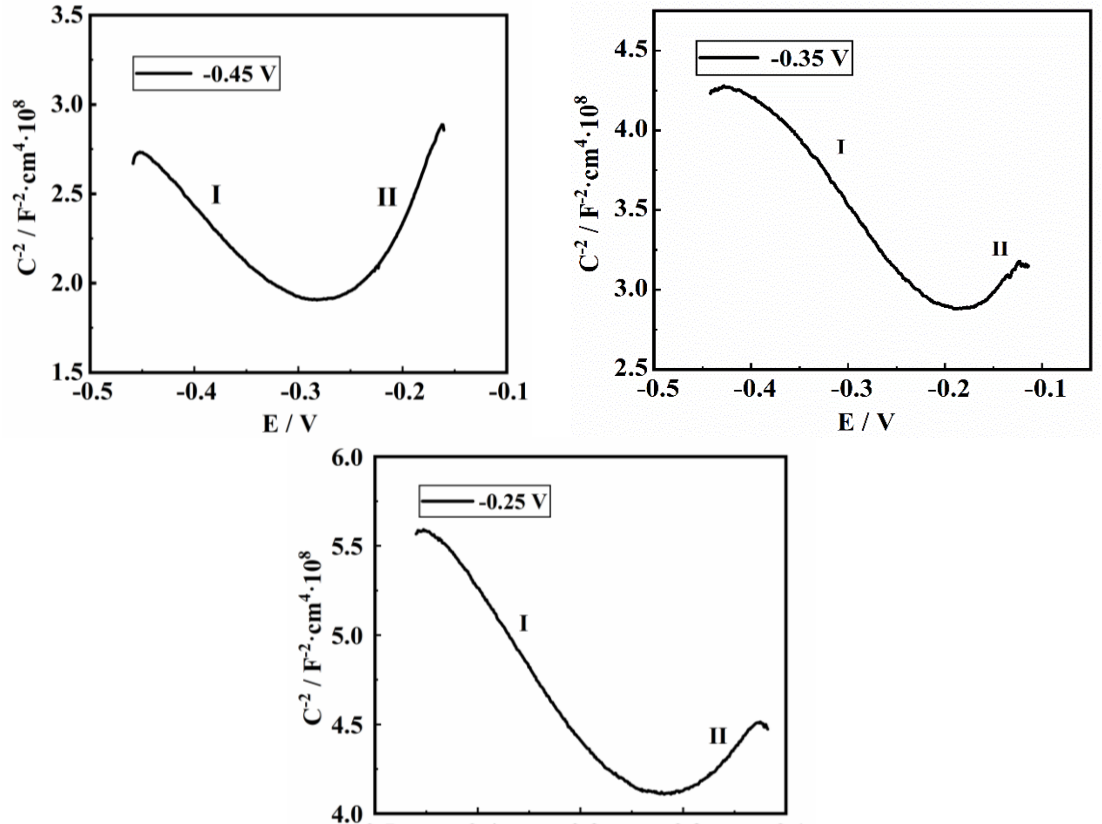

Figure 13. Mott-Schottky curves of passivation film of 13Cr Steel at different potentials for 2 hours.

Fig. 13 shows the Mott-Schottky curve of the 13Cr steel passivated at different potentials for 2 hours and then measured at 1k Hz. According to the positive and negative slope of the M-S curve, the M-S curve was divided into region I and region II. The passive film on the surface of the new 13Cr steel had different semiconductor characteristics in different regions. The slope of the M-S- curve of the 13Cr steel was negative in region I, which indicated that the semiconductor characteristic of the passivation film served as a p-type semiconductor in this potential range, and it was positive in region II, which indicated that the semiconductor characteristic of the passivation film was n-type semiconductor in this potential range.

The semiconductor features of the passivation film are mainly related to the composition and structure of the passivation film. The passivation film on stainless-steel surface is mainly composed of chromium oxides and iron oxides[36,45]. The passivation film formed on the iron surface is a n-type semiconductor, and that formed on the chromium surface is a p-type semiconductor. In region I, the space charge layer in the chromium oxides part was depleted, while that in the iron oxides part was enriched, which was equivalent to a conductor. At this time, the distance between the excess potential and the solution charge of the film decreased with the increase of the scanning potential, resulting in the decrease of the capacitance with the increase of the scanning potential. Therefore, the slope of the M-S curve in region I was negative indicate that the passivation film is a p-type semiconductor. On the contrary, in region II, the space charge layer of the chromium oxide part was in the enrichment state, which was equal to a conductor, while that of the iron oxide part was in the depletion state. At this time, the difference between the excess potential and the solution potential of the film increased with the increase of the scanning potential, which led to the increase of the capacitance with the increase of the scanning potential. Therefore, the Mott-Schottky curve slope in region II was positive, and the film was a n-type semiconductor.

Table 7. Donor/acceptor densities of passivation films on the 13Cr Steel after polarization for 2hours at different potentials.

Potential/V	N_a	N_d
-0.45	1.125E-9	5.286E-10
-0.35	8.868E-10	5.151E-10
-0.25	8.009E-10	4.964E-10

The donor density and acceptor density of the passivation film at different potentials were calculated, and the calculation results are shown in Table 7. The donor density and acceptor density both decreased with the increase of the film potential[46,47]. In general, the lower the donor density or acceptor density is, the better the stability of the passivation film structure is[48,49]. This is because with the decrease of donor density or acceptor density of passivation film, the vacancy of oxygen and metal ion in the passivation film decrease. These vacancies were the important factors leading to pitting corrosion of passive film. Therefore, the structure of the passivation film was more stable by increasing the film potential, which was consistent with the conclusion of EIS.

3.4.2 XPS analysis of passive film

Due to the composition and structure of the passivation film affects the semiconductor characteristics of the passivation film, the chemical composition of the passivation film was analyzed by

XPS. At 90°C, the surface of 13Cr Steel has high passivation ability, and the main component of surface film is Cr_2O_3[50]. Fig. 14 shows the XPS analysis spectra of the passivation film formed on the 13Cr steel after 8 hours at -0.35V, and Table 8 shows the comparison between the standard data and the experimental data of the compound binding energy in the passivation film on the sample surface. It can be concluded from Table 8 that in the passive film on the surface of the 13Cr steel, Cr was in the form of Cr_2O_3 and Fe was in the form of Fe_2O_3.

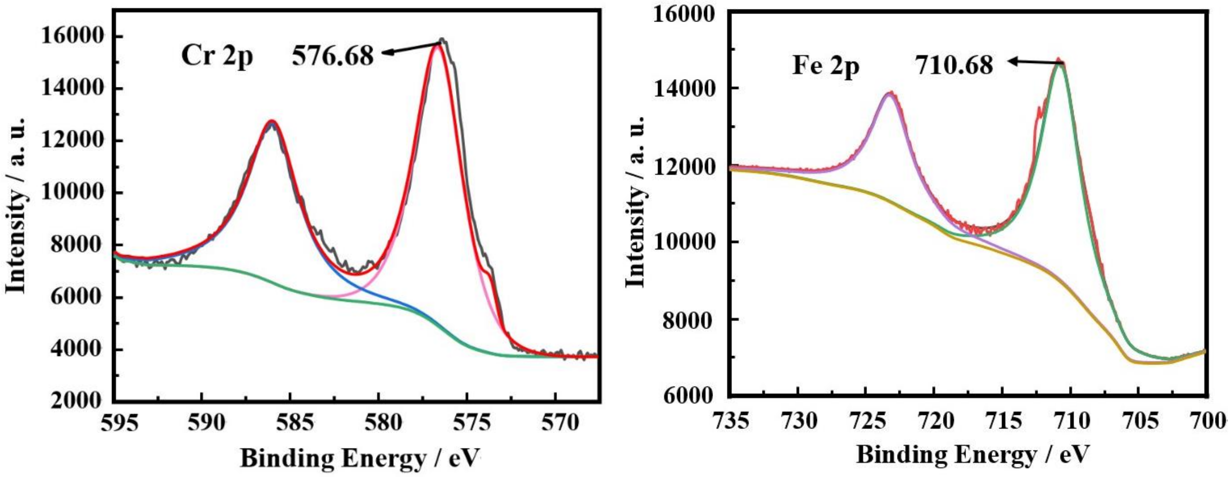

Figure 14. XPS analysis of passivation film on 13Cr Steel after 8 hours at -0.35v.

Table 8. Experimental data and standard data of binding energy of Cr and Fe compounds.

		$Fe_{2p3/2}$	$Cr_{2p3/2}$
standard value	FeO	709.6	
	Fe_2O_3	710.9	
	Cr_2O_3		576.6
	$Cr(OH)_3$		577.3
experimental value	film	710.68	576.68

4. CONCLUSIONS

- There was an obvious passivation region in the potentiodynamic polarization curves of the 13Cr steel, and the electrochemical impedance spectra showed the characteristics of the double capacitive arc. The addition of CO_2 reduced the charge transfer resistance and passivation film resistance, thus reducing the protection of the product film, and significantly improving the corrosion rate.
- With the increase of the Cl^- concentration, the pitting potential of the potentiodynamic polarization curves of the 13Cr steel decreased, the passivation zone decreased, the passivation current

density increased, and the pitting sensitivity increased. The film resistance and charge transfer resistance of the corrosion products decreased first and then increased, resulting in the corrosion rate increasing first and then decreasing.

- The pitting susceptibility of the 13Cr steel increased with the increase of the temperature. EIS exhibited the characteristics of the dual capacitive impedance arc at different temperatures. With the increase of the temperature, the film resistance and charge transfer resistance of the corrosion products first decreased and then increased, the corrosion rate of the 13Cr steel first increased and then decreased.
- The layer of the n-p type semiconductor passivation film was formed on the 13Cr steel in the NaCl solution saturated with CO_2. With the increase of the film potential, the steady-state current density decreased, the charge transfer resistance and the passive film resistance increased, the donor density and acceptor density of the passivation film decreased, the protective performance of the passivation film on the substrate was increased, and corrosion resistance was improved.

ACKNOWLEDGEMENTS
The authors acknowledge the Shaanxi Province for Joint fund project (project 2019JLM-45).

References

1. D. Sidorin, D. Pletcher, B. Hedges, *Electrochim. Acta*, 50 (2005) 4109.
2. H. Ma, *Corros. Prot.*, 34 (2013) 819.
3. F. Zhao, H. Lv, Y. Li, Y. Xue, *Corros. Prot.*, 40 (2019) 925.
4. S. Guo, L. Xu, L. Zhang, W. Chang and M. Lu, *Corros. Sci.*, 63 (2012) 246.
5. S. Hassani, T.N. Vu, N.R. Rosli, S.N. Esmaeely and Y.-S. Choi, *Int. J. Greenhouse Gas Con.*, 23 (2014) 30.
6. Y. Hua, R. Jonnalagadda, L. Zhang, A. Neville and R. Barker, *Int. J. Greenhouse Gas Con.*, 64 (2017) 126.
7. Y. Hua, S. Mohammed, R. Barker, A. Neville, *J. Mater. Sci. Technol.*, 41 (2020) 21.
8. W. Li, L. Xu, L. Qiao, J. Li, *Appl. Surf. Sci.*, 425 (2017) 32.
9. L.D. Paolinelli, B. Brown, S.N. Simison, S. Nesic, *Mater. Chem. Phys.*, 136 (2012) 1092.
10. G. Svenningsen, B.H. Morland, A. Dugstad, B. Thomas, *Eng. Proc.*, 114 (2017) 6778.
11. B. Wang, L. Xu, J. Zhu, H. Xiao and M. Lu, *Corros. Sci.*, 111 (2016) 711.
12. L. Xu, S. Guo, W. Chang, T. Chen and L. Hu, *Appl. Surf. Sci.*, 270 (2013) 395.
13. X. Yue, L. Zhang, Y. Wang, S. Xu and C. Wang, *Corros. Sci.*, 163 (2020) 108277.
14. Y. Zhao, W. Liu, Y. Fan, E. Fan and B. Dong, *Corros. Sci.*, 168 (2020) 108591.
15. M. Xu, Q. Zhang, Z. Wang, J. Liu and Z. Li, *Int. J. Greenhouse Gas Con.*, 71 (2018) 194.
16. L. Xu, B. Wang, J. Zhu, W. Li and Z. Zheng, *Appl. Surf. Sci.*, 379 (2016) 39.
17. Y. Hua, A. Shamsa, R. Barker, A. Neville, *Appl. Surf. Sci.*, 455 (2018) 667.
18. S. Guo, L. Xu, L. Zhang, W. Chang and M. Lu, *Corros. Sci.*, 110 (2016) 123.
19. X.W. Lei, Y.R. Feng, A.Q. Fu, J.X. Zhang and Z.Q. Bai, *Eng. Fail. Anal.*, 50 (2015) 62.
20. K. Krishna Kumar, J. Anburaj, R. Dhanasekar, T. Satishkumar and J. Abuthakir, *J. Mater. Eng. Perform.*, 29 (2020) 6044.
21. Y. Li, M. Chen, J. Li, L. Song and X. Zhang, *Int. J. Miner., Metall., and Mater.*, 25 (2018) 779.
22. Y.Z. Li, X. Wang, G.A. Zhang, *Corros. Sci.*, 163 (2020) 108290.
23. G. Xiao, S. Tan, Z. Yu, B. Dong and Y. Yi, *Petroleum.*, 6 (2020) 106.
24. S. Suresh, C. Palogi, S. Bera, R. Srinivasan, *Thin Solid Films*, 721 (2021) 138550.

25. Y. Hua, S. Xu, Y. Wang, W. Taleb and J. Sun, *Corros. Sci.*, 157 (2019) 392.
26. F. Chen, X. Lu, X. Zhao, Q. Bai and L. Yan, *Acta Metall. Sin.*, 39 (2003) 848.
27. A. Khavasfar, M.H. Moayed, A.H. Jafari, *Int. J. Eng. Trans. A Basics*, 20 (2007) 35.
28. B.R. Linter, G.T. Burstein, *Corros. Sci.*, 41 (1999) 117.
29. M. Heydari, M. Javidi, *Corros. Sci.*, 61 (2012) 148.
30. H. Mansoori, D. Young, B. Brown, M. Singer, *J. Nat. Gas Sci. Eng.*, 59 (2018) 287.
31. M. Magri, I.G.S. Falleiros, N. Alonso-Falleiros, *Corros.: J. Sci. Eng.*, 55 (1999) 769.
32. J. Banaś, U. Lelek-Borkowska, B. Mazurkiewicz, W. Solarski, *Electrochim. Acta*, 52 (2007) 5704.
33. I. Samusawa, S. Nakayama, *Corros. Sci.*, 159 (2019) 108122.
34. X. Mao, X. Liu, R.W. Revie, Corrosion, 50 (1994) 651.
35. Q. Qu, J. Ma, L. Wang, L. Li and W. Bai, *Corros. Sci.*, 53 (2011) 1186.
36. M. Cao, L. Liu, Z. Yu, L. Fan and L. Ying, *Corros. Sci.*, 133 (2018) 165.
37. J. Han, J.W. Carey, J. Zhang, *J. Appl. Electrochem.*, 41 (2011) 741.
38. N. Cao, *Principles of corrosion electrochemistry (3rd Edition)*, Chemical Industry Press, (2008) Beijing, China.
39. Q.Y. Liu, L.J. Mao, S.W. Zhou, *Corros. Sci.*, 84 (2014) 165.
40. H. Liu, F. Cao, G. Song, D. Zheng and Z. Shi, *J. Mater. Sci. Technol.*, 35 (2019) 2003.
41. M. Gao, X. Pang, K. Gao, *Corros. Sci.*, 53 (2011) 557.
42. L. Zeng, X.P. Guo, G.A. Zhang, H.X. Chen, *Corros. Sci.*, 144 (2018) 258.
43. N.E. Hakiki, *Corros. Sci.*, 53 (2011) 2688.
44. H. Luo, C.F. Dong, K. Xiao, X.G. Li, *Appl. Surf. Sci.*, 258 (2011) 631.
45. Q. Xue, S. Zheng, H. Han, *Corros. Sci. Prot. Technol.*, 25 (2013) 152.
46. C. Man, C. Dong, Z. Cui, K. Xiao and Q. Yu, *Appl. Surf. Sci.*, 427 (2018) 763.
47. Y. Li, Y.F. Cheng, *Appl. Surf. Sci.*, 396 (2017) 144.
48. C. Sunseri, S. Piazza, A.D. Paola, F.D. Quarto, *J. Electrochem. Soc.*, 134 (2019) 2410.
49. D.D. Macdonald, *Electrochim. Acta*, 56 (2011) 1761.
50. H. Zhang, Y.L. Zhao, Z.D. Jiang, *Mater. Lett.*, 59 (2005) 3370.